HYDROLOGICAL PROCESSES
*Hydrol. Process.* **29**, 5071–5087 (2015)
Published online 27 April 2015 in Wiley Online Library
(wileyonlinelibrary.com) DOI: 10.1002/hyp.10482

# Using airborne LiDAR to determine total sapwood area for estimating stand transpiration in plantations

Takami Saito,[1,2]* Kazukiyo Yamamoto,[3] Misako Komatsu,[1] Hiroki Matsuda,[1] Shuji Yunohara,[1] Hikaru Komatsu,[4] Makiko Tateishi,[1] Yang Xiang,[1] Kyoichi Otsuki[1] and Tomo'omi Kumagai[2]

[1] *Kasuya Research Forest, Kyushu University, Fukuoka 811-2415, Japan*
[2] *Hydrospheric Atmospheric Research Center (HyARC), Nagoya University, Nagoya 464-8601, Japan*
[3] *Graduate School of Bioagricultural Sciences, Nagoya University, Nagoya 464-8601, Japan*
[4] *The Hakubi Center for Advanced Research, Kyoto University, Kyoto 606-8302, Japan*

## Abstract:

This study offers an unprecedented opportunity to estimate total sapwood area over an entire catchment ($A_{scat}/A_g$) using small-footprint light detection and ranging technology with a minimal amount of labour in field. Forty-two-year-old plantations of Japanese cypress (Hinoki; *Chamaecyparis obtusa* Sieb. et Zucc.) and Japanese cedar (Sugi; *Cryptomeria japonica* D. Don) vegetated the 2.98 ha experimental catchment. Field observations identified diameter at breast height (DBH) of all trees and produced the relationship between DBH and tree sapwood area ($A_{stre}$). The sum of $A_{stre}$ generated actual values of $A_{scat}/A_g$. For light detection and ranging data analyses, local maximum filtering revealed height of tree apices ($H$) and tree number ($N$) with 9% omission errors. A novel process was developed to identify tree species by their apices based on height of the apices and canopy roughness. Four methods were tested. In Methods A–C, $H$ was converted to $A_{stre}$ directly or via DBH, then, the sum of $A_{stre}$ created $A_{scat}/A_g$. $H$–$A_{stre}$ or $H$–DBH relationships were varied irrespective of labour-intensive measurements, and $A_{scat}/A_g$ was underestimated up to 85% of actual value because of the smaller $N$. On the other hand, in Method D, ready-made stand density management diagrams (SDMDs) overestimated mean DBH. However, a product of overestimated mean $A_{stre}$ and the underestimated $N$ was almost identical to the actual $A_{scat}/A_g$. The estimates were 84% and 95% of the true $A_{scat}/A_g$ in Hinoki and Sugi, respectively, and the former will be more precise if the SDMD is suitable for the site as indicated through sensitivity analysis. Copyright © 2015 John Wiley & Sons, Ltd.

KEY WORDS Japanese cedar; Japanese cypress; local maximum filtering; remote sensing; sapflow measurement; stand density management diagram

*Received 30 May 2014; Accepted 6 March 2015*

## INTRODUCTION

The sapflow technique provides tree water use information at the single-tree scale and is not limited by complex terrain and spatial heterogeneity (Wilson *et al.*, 2001). This technique is well suited for determining the effects of species and size composition on transpiration from a forest catchment (e.g. Wullschleger *et al.*, 2001). Sap flux density from measured trees can be scaled up to the catchment level using Equation (1) (e.g. Pataki and Oren, 2003; Kumagai *et al.*, 2005a)

$$E_{cat} = J_s \times \frac{A_{scat}}{A_g} \quad (1)$$

where $E_{cat}$ is the catchment-scale transpiration ($mm\,d^{-1}$), $J_s$ is the mean sap flux density of measuring trees ($m^3\,m^{-2}\,d^{-1}$), $A_{scat}$ is the total sapwood area in the catchment ($m^2$) and $A_g$ is the horizontal ground area of the catchment (hectare in this study). The scaling procedures need to account for two major sources of error: determinations of $J_s$ and $A_{scat}$. Given that $J_s$ measured in a partial stand is similar to the values of other stands within the catchment (Kumagai *et al.*, 2014), $A_{scat}$ is a strong determinant of $E_{cat}$ (Alsheimer *et al.*, 1998; Zimmermann *et al.*, 2000; Roberts *et al.*, 2001).

Conventionally, $A_{scat}$ has been obtained by summing tree sapwood area ($A_{stre}$) over a catchment, which is

*Correspondence to: Takami Saito, Hydrospheric Atmospheric Research Center (HyARC), Nagoya University, Nagoya 464-8601, Japan.
E-mail: takamihappy@gmail.com

Cumulative sapwood area over a catchment area ($A_{scat}/A_g$) was estimated using small-footprint light detection and ranging (LiDAR) technology. Species were separated employing a novel approach using LiDAR-derived tree height ($H$) and canopy roughness. In the method using ready-made stand density management diagrams (SDMDs), a product of overestimated mean tree sapwood area and the underestimated tree number ($N$) was almost identical to the actual $A_{scat}/A_g$. Coupling LiDAR-derived $H$ and $N$ with SDMDs is a less labour-intensive method for evaluating $A_{scat}/A_g$.

deduced from stem diameter at breast height (DBH) and the relationship between DBH and $A_{stre}$ (Kumagai *et al*., 2005b). Here, DBH was measured for all trees using a labour-intensive sampling campaign in the catchment. On-the-ground field surveys for making forest inventories are time consuming and can be dangerous especially in mountainous plantations. Thus, an alternative approach should be developed for assessing $A_{scat}$ so as to reduce labour costs and cover more extensive areas without degrading estimation accuracy.

Light detecting and ranging (LiDAR) is an 'active' remote sensing technology; the system mounted on airborne platforms emits a radiation signal in the form of frequent, short-duration laser pulses, which illuminate a small spot (footprint diameter $<1$ m) on a target surface (Vierling *et al*., 2008). Small-footprint, discrete-return systems can yield very high-resolution three-dimensional positions of billions of laser pulses that are returned from the forest canopy or ground. Application of LiDAR offers the ability to provide high-resolution topographic maps and highly accurate estimates of vegetation height, cover and canopy structure across broad spatial extents (Lefsky *et al*., 2002; Roth *et al*., 2007; Vierling *et al*., 2008). Thus, LiDAR technology would allow us to evaluate $A_{scat}$ over large plantation areas with minimal effort.

Japanese cypress, *Chamaecyparis obtusa* Sieb. et Zucc. (Hinoki), and Japanese cedar, *Cryptomeria japonica* D. Don (Sugi), are both in the Cupressaceae and thrive as native coniferous species in Japan. Both species are intensively planted for timber production, and plantations of the two species were estimated to occupy approximately 19% of the total land area of Japan in 2007 (Japan Forestry Agency, 2013). Most of these plantations are located on steep slopes in mountainous river headwater regions. Therefore, effective and accurate inventory of the plantations at the catchment scale is a high priority for land managers, who seek to develop adequate land use strategies in mountainous regions where water resource management is of interest (Kumagai *et al*., 2014).

Hinoki and Sugi were frequently planted simultaneously in the same catchment. Empirically based planting techniques suggest Hinoki should be planted at mid-slope locations, while Sugi should be planted on the lower slopes near valleys (e.g. Kawana, 1992; Nagakura *et al*., 2004). However, no studies have separated individual trees detected in LiDAR-derived data sets into Hinoki and Sugi in a mixed plantation. The borderlines between the two species' areas are not always clear, and manual separation in the geographic information system (GIS) is not efficient for processing LiDAR-derived data across a vast plantation area. Thus, automatic processes using algorithms need to be developed for separating Hinoki and Sugi based on the difference in species-specific characteristics in canopy structure detected by means of airborne LiDAR.

This study aimed to produce an innovative scheme to estimate $A_{scat}/A_g$ using small-footprint airborne LiDAR technology that requires only minimal effort related to on-the-ground field observations. $A_{scat}/A_g$ was estimated using four methods that combine LiDAR-derived variables and tree allometry relationships, which were existing or obtained from field measurements. A novel approach enabled separation of tree apices in the LiDAR data into the two species based on differences in a canopy structure. To validate the estimation within a reasonable and practical level of accuracy, the LiDAR-derived $A_{scat}/A_g$ was compared with field-derived $A_{scat}/A_g$. The results provide strategies for hydrological observations, which are required for optimal water resource management in mountainous regions of Japan.

## MATERIALS AND METHODS

### *Study site*

Observations were conducted in the Yayama Experimental Catchment (YEC; 2.98 ha, 33°31′N, 130°39′E, 304.1–405.8 m a.s.l.) in Fukuoka Prefecture in western Japan (Figure 1a). The northeast facing slopes of the catchment serve as the headwaters of the Onga River. A mean annual temperature of 15.6 °C and annual precipitation of 1790 mm averaged over a 30-year period between 1971 and 2010 were recorded at Iizuka meteorological observatory, 15 km north of our site at 37 m a.s.l. A plantation of Hinoki and Sugi covered the entire catchment; these trees were planted in 1969 and 42 years old in January 2011. The site index curves for Hinoki (Japan Forestry Agency, 1957) and Sugi (Inoue and Miyahara, 1954) indicated that the plantation could be categorized as middle to high quality class. The leaf area index has been estimated at 2.8–3.87 $m^2\,m^{-2}$ (Saito *et al*., 2013). Evergreen broad-leaved trees, such as *Eurya japonica* Thunb., covered parts of YEC, but such small trees and shrubs on the forest floor were cleared prior to observations so as to facilitate the field inventory.

### *On-the-ground field observations*

Diameter at breast height (at approximately 1.2 m to 1 mm accuracy) of all trees in the entire area of the YEC was measured using a tree calliper. The DBHs of trees growing on slopes were measured from the tree base on the upper side of the slope. Field inventory was conducted by a team of seven persons for 3 days in 15–17 November 2010. For efficient measurements, the entire area of the YEC was divided into five sub-areas. The team was divided into groups to sample each sub-area. The populations of the plantation trees were estimated as

 

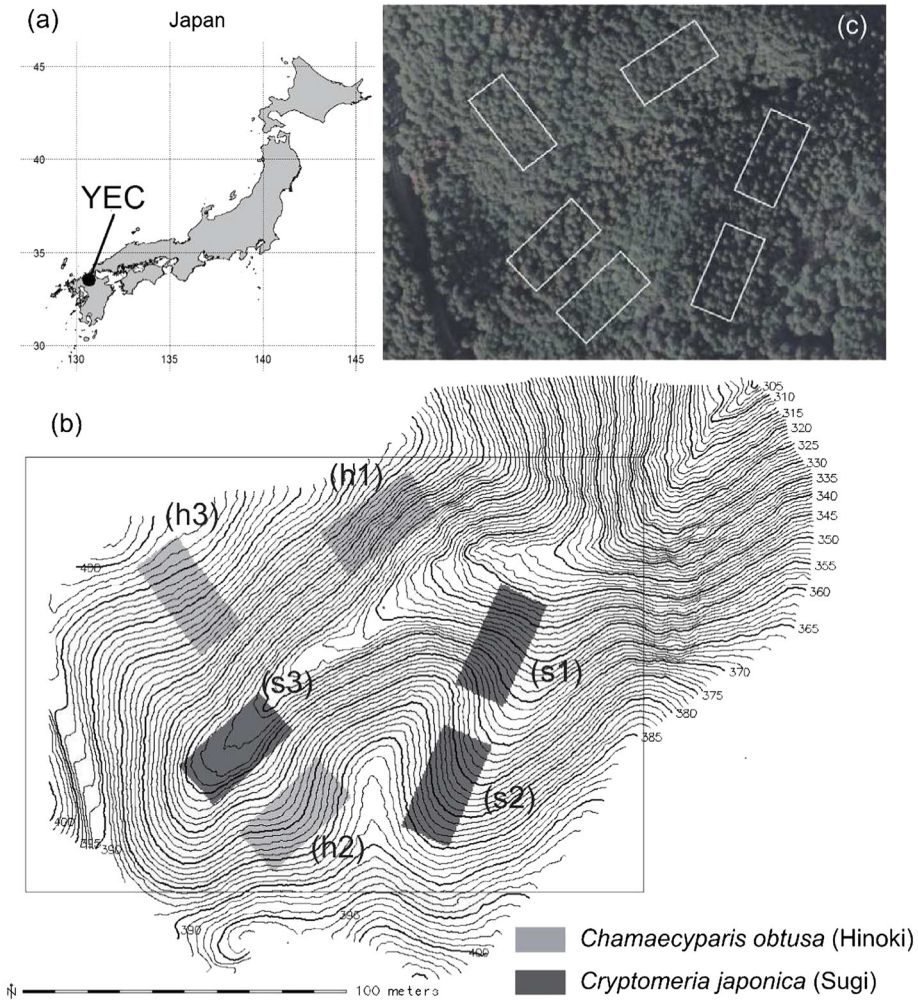


Figure 1. (a) Location map showing the vicinity of the Yayama Experimental Catchment (YEC). (b) Topographical map of the YEC. Thin and thick contours have intervals of 1 and 5 m, respectively. Uniform species windows (USWs) show areas of Hinoki (h1–3, light grey) and Sugi (s1–3, deep grey). (c) Orthophoto of a part of the YEC, the location of which is indicated with a large square in (b). White lines indicate the locations of the USWs. Table III presents topographic parameters of each USW

2645 and 1300 for Hinoki and Sugi, respectively. The mean ± population standard deviation (range) of DBH was 21.8 ± 4.3 cm (5.0–39.7 cm) and 24.4 ± 5.4 cm (8.0–52.6 cm) for Hinoki and Sugi, respectively (Figure 2). Skewness (0.23 and 0.48 for Hinoki and Sugi, respectively) indicated that the DBH distributions had a longer tail to the right (i.e. greater DBH class), but the range of measurements was not far from symmetrical. Kurtosis (0.45 and 0.51 for Hinoki and Sugi, respectively) indicated that the distributions were more peaked than a natural distribution. Skewness and kurtosis of Hinoki were smaller than those of Sugi, which imply that the DBH distribution of the Hinoki population was less skewed and less peaked (i.e. near a normal distribution) than that of the Sugi population.

The relationship between individual tree height ($H$; m) and DBH was obtained from 102 Hinoki and 79 Sugi trees across the entire area of the YEC, and included 3.9% and 6.1% of their populations, respectively. The $H$ of the sampled trees was measured using an ultrasonic hypsometer (Vertex IV, Haglöf, Långsele, Sweden), and simultaneously, their DBH was obtained from taping the circumference at breast height. Most of the measurements were taken in January 2012, and additional measurements were made in July 2013 and April 2014. Some data of $H$ in 2012 were used with DBH obtained in 2010 and 2011. The accuracy of $H$ measurements was confirmed through comparing the $H$ with the tree height measured using a tape ($H_t$; m) of harvested trees. Near linear relationships were found in Hinoki ($n = 10$, $H_t = 0.95H + 1.06$, $R^2 = 0.96$) and Sugi ($n = 12$, $H_t = 0.94H + 0.92$, $R^2 = 0.89$). The measured DBH ($D$; cm) was plotted against $H$ to develop an allometric

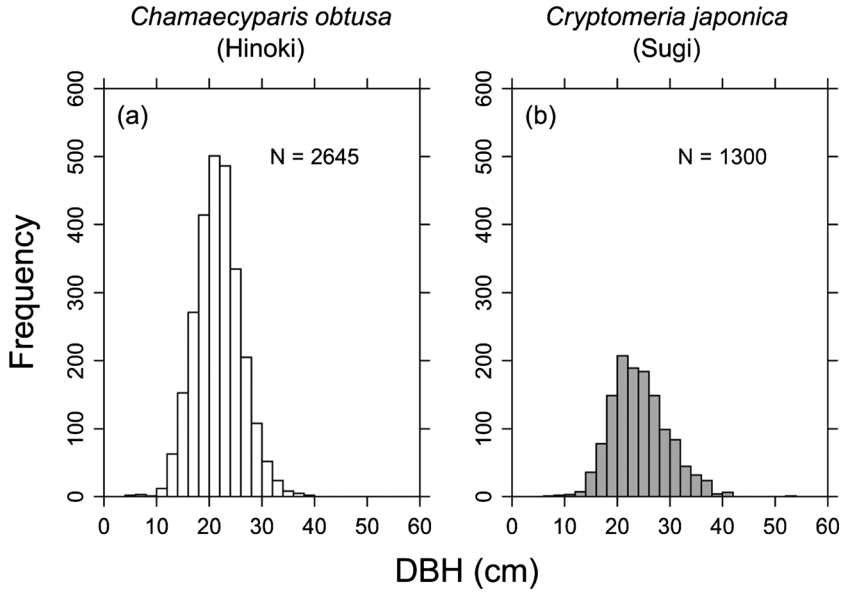


Figure 2. Histogram of diameter at breast height (DBH) for populations of (a) Hinoki and (b) Sugi in the Yayama Experimental Catchment. Data were obtained from field observations

equation that could be used to predict DBH based on $H$ (Figure 3a). An exponential regression curve was applied on the plots for each species as follows:

$$D = a \times H^b \tag{2}$$

*Estimating sapwood area in a stem cross section*

Sapwood depth (SWD; cm) of Hinoki was determined as the width of xylem from just beneath the bark to the heartwood in the stem cross section. The colour difference in the sapwood–heartwood boundary was not clear in some cases. Thus, the width of the wetter part of xylem adjacent to bark, which was visible immediately after sampling, was used for determining SWD. For Sugi, SWD was determined as the width of xylem from just beneath the bark to the heartwood the same as for Hinoki but subtracted by the depth of intermediate wood (10 mm). The heartwood of Sugi had a rich red colour, which was distinct from the intermediate white part of the xylem in the stem cross section. The intermediate wood ('white zone') is the transition zone from sapwood to heartwood, and ray parenchyma begins to die off within that region (Nobuchi and Harada, 1983). The intermediate wood is characterized as low water content (Kuroda *et al*., 2009), high air permeability (Nagai and Taniguchi, 2001), with no water movement confirmed by means of the dye injection method (Ohashi *et al*., 1985; Kumagai *et al*., 2005a). The width is approximately 10 mm (Nobuchi and Harada, 1983; Kumagai *et al*., 2005a; Nagai and Utsumi, 2012).

The SWD and bark depth (BRD; cm) were measured using a ruler on increment borer samples (5 mm in diameter), with bores extracted at breast height from four orthogonal directions of the stem from 2010 to 2012. The SWD and BRD were also obtained from a stem cross section at breast height of harvested trees. The data were collected across the catchment area, immediately after a 50% thinning operation in February 2012. Missing BRDs were estimated using the relationship between DBH and BRD. As a result, the total number of trees sampled for SWD was 119 for Hinoki and 59 for Sugi. No significant differences in mean SWD or mean BRD were observed among the four directions ($P > 0.65$; ANOVA) for either species; therefore, the outer and inner circumferences of sapwood in stem cross sections could be treated as perfect circles. This resulted in a successful calculation of tree sapwood area ($A_{\mathrm{stre}}$; $\mathrm{m}^2$) by applying the equation $A_{\mathrm{stre}} = L_{\mathrm{SWD}} \times \pi \times [(D - 2L_{\mathrm{BRD}}) - L_{\mathrm{SWD}}]$, where $L_{\mathrm{SWD}}$ and $L_{\mathrm{BRD}}$ represent SWD and BRD, respectively. Then, the allometric relationship between DBH and $A_{\mathrm{stre}}$ for each species was obtained through fitting an exponential equation as follows (Figure 4):

$$A_{\mathrm{stre}} = m \times D^n \tag{3}$$

The $A_{\mathrm{stre}}$ was plotted against $H$ to develop an allometric equation that could be used to predict $A_{\mathrm{stre}}$ based on $H$ (Figure 3b). The equation fitted on this $H$–$A_{\mathrm{stre}}$ relationship was

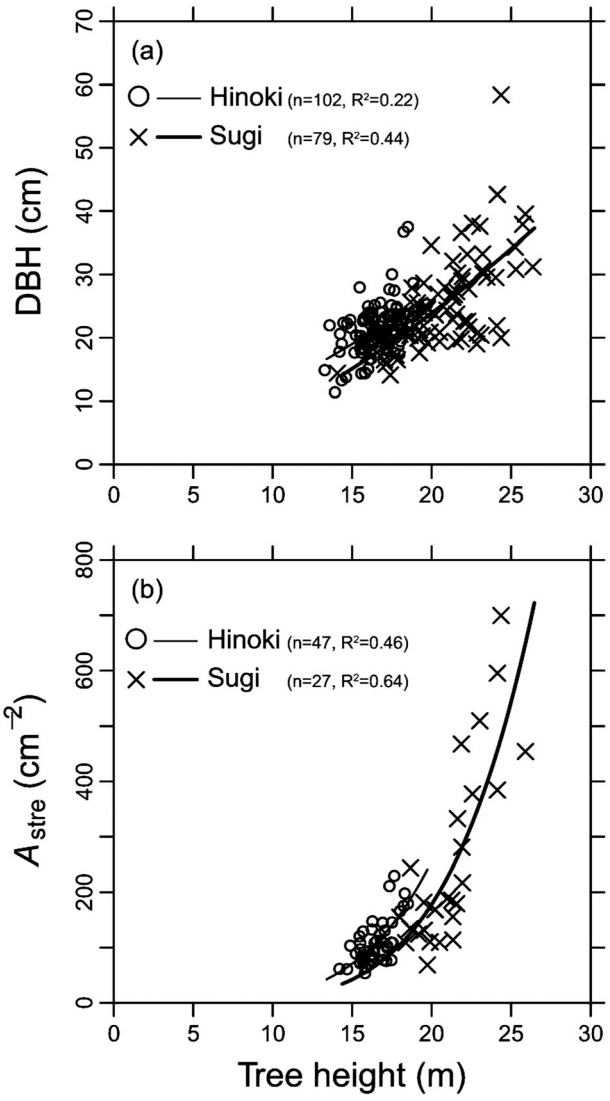


Figure 3. Relationships between tree height and (a) diameter at breast height (DBH) or (b) tree sapwood area ($A_{stre}$) for sample trees based on field observations. Species are *Chamaecyparis obtusa* (Hinoki) and *Cryptomeria japonica* (Sugi). The range of tree heights in the curve fitting was 13.4–19.7 m for Hinoki and 14.4–26.5 m for Sugi. The ranges were the minimum and maximum height of the tree apex in the catchment detected using the LiDAR technique for each species. Table I shows the parameters of the regression curves

$$A_{stre} = q \times H^r \quad (4)$$

Table I summarizes the parameters and coefficients of determination of Equations (2), (3) and (4).

*Creating digital models from LiDAR data*

The airborne LiDAR data were acquired by Aero Asahi Corporation (Tokyo, Japan) 4 months after the on-the-ground tree census. Table II summarizes the system and settings of the LiDAR observations. The laser scanner emitted near-infrared laser pulses and received the returned first and last pulses that were stronger than the trigger level. The elapsed time between pulse emission and detection produced the round-trip distance between the LiDAR system and the target object (Roth *et al.*, 2007; Hirata *et al.*, 2009). The position of the platform was monitored with the aide of an onboard global positioning system, being standardized at a nearest global positioning system standard point on the ground (33°34′47″N, 130°40′32″E, 44.37 m a.s.l.). Simultaneously, an inertial measurement unit reported the attitude (roll, pitch and yew) of the LiDAR sensor. Combining this information with a precise time reference, each source of data yields the absolute position of the reflecting surface for each laser pulse.

The pulse laser beam was applied orthogonal to the helicopter track, so that the sampled points fell across a wide band or swath along the track, which can be gridded into an image. The entire research area including the YEC was surveyed using seven parallel flight lines with regular intervals, oriented NE–SW. The scanned band of 130 m in width overlapped 48% between adjacent swaths to ensure the accuracy of the combined scanned data of the flying courses. The maximum difference was 0.06 m in the overlapped sub-areas between the flight courses.

Knowing the number of trees ($N$) and their $H$ is essential to the LiDAR estimation of $A_{scat}$. For this process, LiDAR-derived digital terrain (DTM) and digital surface (DSM) models were created as 0.5-m gird-sized raster data sets. Processing and analysing of the raster data were conducted on the open source software suite GIS (GRASS GIS 6.4.3, GRASS Development Team, 2012). The DTM was generated from the last returns of the laser pulses as a raster data set by Aero Asahi Corporation. Two types of DSM were created from the first returns of the laser pulses. $DSM_{max}$ was composed of the grids with surface elevation obtained from the maximum value of dispersed points falling in each grid, and was used for detecting tree apices. $DSM_{mean}$ were composed of the grids with the mean elevation of the dispersed points, and were used for extracting the hypothetical canopy of each tree apex. Raw data of both DSMs included blank grids (0.7% of all grids), which were interpolated with a 'bicubic' method. The raster layers of the DTM, the DSMs and orthophoto were superimposed using GRASS software, and a rectangle workspace (399.5 × 409.5 m) that included the entire area of the YEC was created. The catchment area of the YEC was estimated to be 3.0153 ha based on the DTM, after inputting the coordinates of the weir (33°31′0.6″N, 130°39′19.1″E). The LiDAR-derived boundary of the YEC reasonably corresponded with the boundary of the catchment delineated in the field inventory.

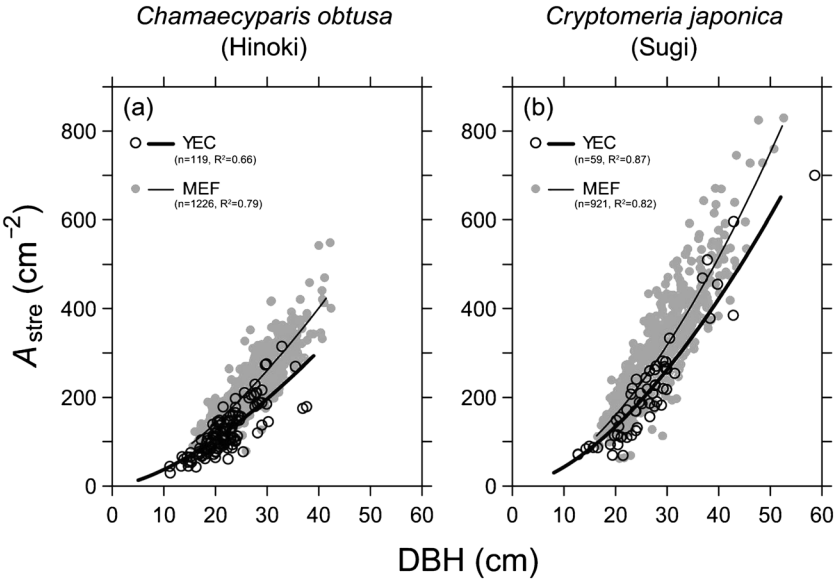


Figure 4. Tree sapwood area in a stem cross section ($A_{stre}$) plotted against diameter at breast height (DBH) for sample trees based on field observations. The points of the Yayama Experimental Catchment (YEC) were imposed on the points of the Miyazaki Experimental Forest (MEF) from Kumagai *et al*. (2005b). For YEC, the range of DBH in the curve fitting was 5.0–39.7 m for Hinoki and 8.0–52.6 m for Sugi. The ranges were the minimum and maximum DBH in the catchment based on field observations. Table I shows the parameters of the regression curves

Table I. Parameters for regression curves

| Equation | Equation number | Parameter | *Chamaecyparis obtusa* (Hinoki) | *Cryptomeria japonica* (Sugi) |
|---|---|---|---|---|
| $D = a \times H^b$ | (2) | $a$ | 0.77 | 0.20 |
| | | $b$ | 1.19 | 1.59 |
| $A_{stre} = m \times D^n$ | (3) | $m$ | 1.11 | 0.96 |
| | | $n$ | 1.52 | 1.65 |
| | (3)* | $m$ | 1.59 | 1.02 |
| | | $n$ | 1.50 | 1.69 |
| $A_{stre} = q \times H^r$ | (4) | $q$ | 3.89E−04 | 5.47E−05 |
| | | $r$ | 4.47 | 5.01 |

$D$ is diameter at breast height (m), and $H$ is tree height (m).
$A_{stre}$ is sapwood area in a stem cross section ($m^2$).
*Equation (3) is for the Miyazaki Experimental Forest in Kumagai *et al*. (2005b).

Table II. Settings of the LiDAR system

| Parameter | Performance |
|---|---|
| Measurement date | 5 and 10 March 2011 |
| Platform | Helicopter |
| Flying speed and altitude | 90 km h$^{-1}$, 500 m |
| Sensor | OPTEC ALTM3100G4 |
| Laser wavelength | 1064 nm |
| Laser pulse frequency | 100 000 Hz |
| Scan frequency | 40 Hz |
| Scan angle | 28° |
| Beam divergence | 0.3 mrad |
| Footprint diameter | 0.11 m |
| Laser sampling density | 30 points m$^{-2}$ |

Using remotely sensed data, all trees in the YEC were partitioned into two species based on the characteristics detected in the uniform species windows (USWs: Figure 1b and c) in the DSMs. Each USW is an approximately 16.2 × 33.2 m rectangle, and total areas of the three USWs for each of the two species were almost the same. The superimposed orthophoto allowed us to confirm that each USW represents a single species, i.e. Hinoki or Sugi. The criteria used for species confirmation was: Hinoki crowns that were deep green, relatively flat and had a continuous shape. In comparison, Sugi crowns were red to brown in March and had a clearly shaded area. The three USWs were established in locations representing various topographies of the YEC. Table III

Table III. Results of calculations on DTM and DSMs in the catchment and in the uniform species windows

| | | | | *Chamaecyparis obtusa* (Hinoki) | | | | *Cryptomeria japonica* (Sugi) | | | | All USWs |
|---|---|---|---|---|---|---|---|---|---|---|---|---|
| | | | | USW | | | Subtotal | USW | | | Subtotal | Total |
| Value | Calculation | Unit | Catchment | h1 | h2 | h3 | | s1 | s2 | s3 | | |
| **DTM** | | | | | | | | | | | | |
| Area | | $m^2$ | 30 153 | 532.25 | 541.5 | 538 | 1611.75 | 539.75 | 539.25 | 544.5 | 1623.5 | 3235.25 |
| Elevation | Min_Max | m | 304.1_405.8 | 363.4_383.0 | 375.8_387.2 | 380.2_398.6 | 363.4_398.6 | 350.3_373.7 | 370.3_386.6 | 364.4_372.1 | 350.3_386.6 | 350.3_398.6 |
| | Difference | m | 101.6 | 19.6 | 11.5 | 18.4 | 35.2 | 23.5 | 16.3 | 7.8 | 36.3 | 48.3 |
| Slope | Mean | Degree | 32 | 43 | 28 | 27 | 33 | 32 | 27 | 19 | 26 | 29 |
| Aspect | Mean | Degree | 175 | 135 | 286 | 147 | 190 | 41 | 61 | 196 | 99 | 144 |
| Roughness | Mean | m | 0.8 | 1.3 | 0.6 | 0.7 | 0.9 | 0.8 | 0.6 | 0.5 | 0.6 | 0.7 |
| **$DSM_{max}$** | | | | | | | | | | | | |
| Tree number | | Trees | 3582 | 77 | 76 | 83 | 236 | 58 | 67 | 55 | 180 | 416 |
| Tree density | | Trees $ha^{-1}$ | 1188 | 1447 | 1404 | 1543 | 1464 | 1075 | 1242 | 1010 | 1109 | 1286 |
| Tree height | Min_Max | m | 13.4_26.5 | 15.3_19.3 | 14.4_17.9 | 13.4_17.7 | 13.4_19.3 | 15.2_23.6 | 17.5_23.2 | 19.2_26.2 | 15.2_26.2 | 13.4_26.2 |
| | Mean ± SD | m | 17.9 ± 2.5 | 17.2 ± 1.0 | 16.5 ± 0.8 | 15.5 ± 0.8 | 16.4 ± 1.1 | 19.9 ± 1.9 | 20.2 ± 1.6 | 23.1 ± 1.7 | 21.0 ± 2.2 | 18.4 ± 2.8 |
| **$DSM_{mean}$** | | | | | | | | | | | | |
| $\sigma$ | Min_Max | m | 0.2_6.5 | 0.4_1.5 | 0.3_1.6 | 0.3_1.1 | 0.3_1.6 | 0.5_2.7 | 0.4_2.2 | 0.5_5.6 | 0.4_5.6 | 0.3_5.6 |
| | Mean ± SD | m | 1.0 ± 0.7 | 0.7 ± 0.2 | 0.6 ± 0.2 | 0.6 ± 0.2 | 0.6 ± 0.2 | 1.1 ± 0.4 | 1.1 ± 0.4 | 1.3 ± 0.8 | 1.2 ± 0.6 | 0.9 ± 0.5 |

DTM, digital terrain model; DSM, digital surface model; USW, uniform species window on DSMs for species separation; SD, sample standard deviation.
$DSM_{max}$ and $DSM_{mean}$ are the DSMs composed of grids with the highest and mean value among the first returns of the laser pulse fallen in each grid, respectively.
Location of USW h1–3 of Hinoki is indicated by light grey area (h1–3), and location of USW s1–3 of Sugi is indicated by deep grey area (s1–3) in Figure 1, respectively.
Roughness is the difference between the maximum and the minimum value in a group of nine grids, including a cell and the eight surrounding grids in DTM.
$\sigma$ is population standard deviation of the height of 29 grids in the hypothetical canopy circle, including a grid of local maximum and its 28 surrounding grids in the $DSM_{mean}$.

showed the topographic features of the YEC and the USWs analysed with an algorism using the 'kmeans' and the 'terrain' command of the 'raster' package in the R 3.0.2 (R Core Team, 2013).

*Tree apex identification in the digital surface model*

The local maximum filtering (LMF) technique was applied to detect the location and height of tree apices in the $DSM_{max}$ (Hyyppä *et al.*, 2001; Takahashi *et al.*, 2005). LMF is based on the assumption that the highest laser reflectance in the neighbourhood represents the tip of a tree crown. LMF works best for detecting trees with a single and well-defined apex, such as coniferous species (Popescu *et al.*, 2002). The algorithm for LMF used the 'focal' command of R. The moving window size used fixed $3 \times 3$ grids (i.e. $1.5 \times 1.5$ m) and inspected entire grids in the $DSM_{max}$ of the workspace. The algorithm outputs the coordinate and elevation of a grid, if the grid was higher than the surrounding eight grids in the window. The LiDAR-derived $H$ was obtained by subtracting the DTM from $DSM_{max}$ levels of the tree apices. The threshold value for $H$ (13.4 m) was determined from the minimum level of $H$ in all USWs (Table III), which was almost identical to the minimum $H$ found in field surveys (13.2 m, Figure 3a).

*Methods to evaluate $A_{scat}/A_g$*

Four methods are proposed for evaluating $A_{scat}$ based on the LiDAR data. Figure 5 provides a flow chart of processes so as to calculate $A_{scat}$, and Table IV shows the parameters used. The method field-derived $A_{scat}/A_g$ (Field) generated the reference of $A_{scat}/A_g$; each tree's DBH in the field inventory was converted to each $A_{stre}$ using the DBH–$A_{stre}$ relationships (Equation [3] and Figure 4). The $A_{stre}$ of all trees was summed over the entire YEC and assigned as $A_{scat}$, which was divided by the 2.98 ha catchment area.

Four LiDAR approaches were employed to estimate $A_{scat}/A_g$ in the LiDAR-derived catchment area (3.0153 ha). Methods A–C required the LiDAR-derived $H$ and field-derived equations to estimate $A_{stre}$, while Method D used only the LiDAR-derived $H$ and $N$ and the 'ready-made' diagrams. Method A was the most direct approach, where LiDAR-derived $H$ of each tree was converted to each $A_{stre}$ using Equation (4); then the measures of $A_{stre}$ were summed and denoted as $A_{scat}$ for all trees identified through LMF.

Equation (4) used for Method A is difficult to obtain in the plantations because of stem injuring. Method B used conventional relationships of $H$–DBH (Equation [2]) and DBH–$A_{stre}$ (Equation [3]) to estimate $A_{stre}$ from each tree's

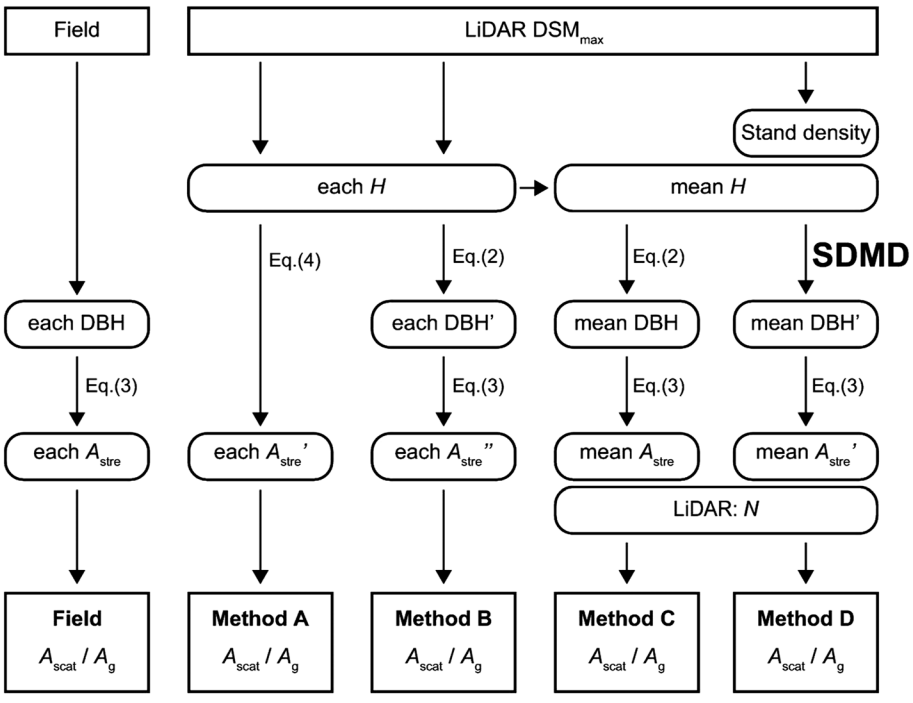


Figure 5. Flow chart of calculation processes to estimate the cumulative catchment sapwood area divided by the ground area ($A_{scat}/A_g$). The field-derived $A_{scat}/A_g$ (Field) was used as a reference value for the other four LiDAR-derived $A_{scat}/A_g$ (Methods A–D). Abbreviations are tree sapwood area ($A_{stre}$), the digital surface model composed of the grids with the maximum level of the pulse falling in each grid ($DSM_{max}$), diameter at breast height (DBH), height of a tree apex ($H$), number of trees apices ($N$) and stand density management diagram (SDMD)

Table IV. Total sapwood area over the catchment area estimated by a field method and four LiDAR methods

| | | *Chamaecyparis obtusa* (Hinoki) | | | | | *Cryptomeria japonica* (Sugi) | | | | |
|---|---|---|---|---|---|---|---|---|---|---|---|
| | | | Method | | | | | Method | | | |
| Parameter | Unit | Field | A | B | C | D | Field | A | B | C | D |
| Tree density | Trees ha$^{-1}$ | — | — | — | — | 1464 | — | — | — | — | 1109 |
| Mean $H$ | m | — | — | — | 16.7 ± 1.4 | 16.7 ± 1.4 | — | — | — | 20.3 ± 2.6 | 20.3 ± 2.6 |
| Mean DBH | cm | 21.8 ± 4.3 | — | 21.6 ± 2.2 | 21.6 | 20.9 | 24.4 ± 5.4 | — | 24.6 ± 4.9 | 24.4 | 26.0 |
| Mean $A_{stre}$ | cm$^2$ tree$^{-1}$ | 122.9 ± 36.8 | 121.5 ± 46.0 | 120.2 ± 18.5 | 119.6 | 113.5 | 191.0 ± 70.1 | 219.9 ± 121.0 | 192.9 ± 60.2 | 186.5 | 207.3 |
| Tree number | Trees | 2645 | 2437 | 2437 | 2437 | 2437 | 1300 | 1145 | 1145 | 1145 | 1145 |
| $A_{scat}/A_g$ | m$^2$ ha$^{-1}$ | 10.9 | 9.8 | 9.7 | 9.7 | 9.2 | 8.3 | 8.3 | 7.3 | 7.1 | 7.9 |

$H$, tree height; DBH, diameter at breast height; $A_{stre}$, sapwood area in a stem cross section; $A_{scat}/A_g$, cumulative sapwood area divided by ground area in the catchment.
Number with ± operator indicates mean ± population standard deviation.
Methods are referred to Figure 5.

LiDAR-derived $H$. The plots of $H$–DBH were scattered (Figure 3a), indicating that the DBH estimation for each tree was not necessarily accurate. Method C replaced each tree's $H$ by an averaged $H$ and determined mean DBH and mean $A_{stre}$ using Equations (2) and (3), respectively. In Methods C and D, the $A_{scat}$ was given based on a product of the mean $A_{stre}$ and $N$ obtained with LMF.

Method D also used the $H$ averaged over the tree apices identified using LMF and included an additional parameter, stand density in the USWs. These two parameters were applied to a stand density management diagram (hereinafter, SDMD), estimating the catchment mean DBH for each species. Then, the mean DBH was converted to the mean $A_{stre}$ through Equation (3), yielding $A_{scat}$ as stated earlier.

The SDMD (Ando, 1968) is an average stand-level model, which graphically predicts mean DBH and yield volume from the tree density and height in monoculture tree plantations, throughout all stages of stand development. The theoretical background for SDMD is the reciprocal equations of the competition-density and yield-density effects, and the self-thinning rule, which were found in even-aged monospecific plant population after long-term intraspecific competition (Kira *et al.*, 1953). SDMDs have been developed for some commercially important species, and region-specific SDMDs cover major plantation sites across Japan. Newton (1997) reviewed the application of the SDMD to various tree species in other countries. In this study, stand mean DBH of Hinoki and Sugi were deduced with SDMDs for the Kyushu area using the spreadsheet software produced by the Forestry and Forest Products Research Institute of Japan (http://www.ffpri.affrc.go.jp/database/yieldindex/index.html; in Japanese).

## RESULTS

### *Species identification for tree apices in LiDAR data*

A hypothetical canopy circle, centred on the coordinates of each tree apex detected with LMF, was established for each tree in the $DSM_{mean}$ across the workspace. The radius ($r$) of the circle was determined as 1.57 m using the equation; $r = [A_{plot}/(\pi \times N_{plot})]^{0.5}$, where $A_{plot}$ is total area (3235.25 m$^2$) and $N_{plot}$ was the total number of trees (416 trees) in the six USWs (Table III). Each circle contained the centre points of 29 grids, which composed a population of surface elevations that could be used to derive the population standard deviation ($\sigma$) within the circle (i.e. each tree crown's continuum). The $\sigma$ was calculated using the 'extract' command of R, and the circle radius was adjusted with a 'buffer' parameter. Note that lower values of $\sigma$ are assumed to represent relatively flat canopy shapes with dense leaves (Hinoki-like), which

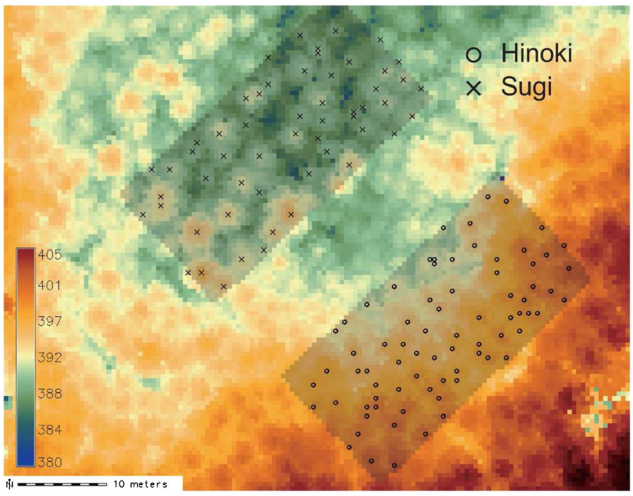


Figure 6. Digital surface model, which is composed of surface elevation grids obtained from the maximum value of dispersed points falling in each grid ($DSM_{max}$). Right and left shaded areas indicate the uniform species windows (USWs) of *Chamaecyparis obtusa* (Hinoki) and *Cryptomeria japonica* (Sugi), which are shown as h2 and s3 in Figure 1b, respectively. The points indicate local maxima detected with local maximum filtering

are continuous to neighbouring trees. Conversely, the higher values of $\sigma$ would represent relatively conical crown shapes with clumped leaves (Sugi-like), which are isolated from neighbouring trees. The data set for each tree apex including the coordinates, $H$, and $\sigma$ were prepared across the entire area of the workspace. Next, the tree apices in the catchment or each USW were extracted based on the coordinates of those areas in the DTM. Thus, grids outside the area beside the edges were included for detecting tree apices using LMF and for calculating $\sigma$ in the canopy circle. Figure 6 showed that the LiDAR-derived local maxima succeeded in identifying the tops of mounds in $DSM_{max}$ (i.e. tree apices).

Figure 7 shows the frequency distributions of the $H$ and $\sigma$ for each species in the USWs, revealing a novel distinction between Hinoki and Sugi crown characteristics. All the tree apices in the three USWs of each species were aggregated, and threshold values were obtained from the mean ± three sample standard deviations of $H$ and $\sigma$ (Table III). We noted that trees with $H > 19.7$ m

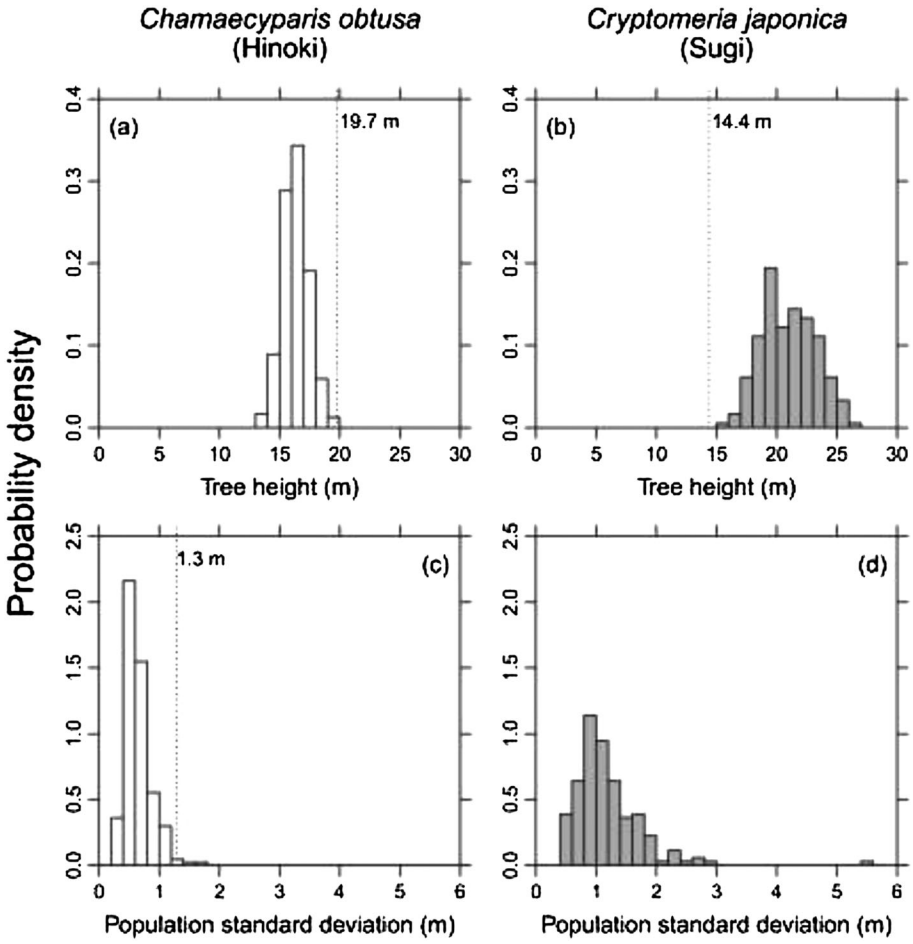


Figure 7. (a, b) Histograms for height of the tree apex ($H$), and (c, d) those for the population standard deviation ($\sigma$) of 29 levels of grids within a hypothetical canopy circle (1.57 m in radius). Data were obtained from uniform species windows for Hinoki (a, c) and Sugi (b, d). $H$ and $\sigma$ were obtained in the digital surface model composed of the maximum ($DSM_{max}$) and mean ($DSM_{mean}$) pulse level in each grid, respectively. Vertical dots with numbers indicate threshold values for separating the species (mean ± three sample standard deviations)

could be classified as Sugi trees in the USWs. An overlap was observed between Hinoki and Sugi in $H > 14.4$ m. However, we also noted that all trees with $H > 14.4$ m and $\sigma > 1.3$ m could be classified as Sugi. Any other trees that did not meet these criteria could be classified as Hinoki trees. In addition, some tree apices (28.3% of total) in the USWs of Sugi were in the class of Hinoki (i.e. $H \leq 19.7$ m and $\sigma \leq 1.3$ m).

Combination of the LMF technique and the criteria for species detection allowed us to create a map for distribution of all 'estimated' Hinoki and Sugi tree apices in the YEC (Figure 8). A total of 3582 tree apices were identified; in other words, 90.8% of 3945 field-verified 'actual' trees were identified using LMF. The numbers of the LiDAR-identified Hinoki and Sugi were 2437 and 1145, respectively (Table IV), which represented 92.1% and 88.1% of their actual populations. Note that the distribution of the species was consistent with traditional forestry guidelines (i.e. planting Hinoki trees on the middle of the slope and Sugi trees in the valley).

### *LiDAR-derived total sapwood area over the catchment area*

Figure 9a and b shows the frequencies of LiDAR-derived $H$ in the catchment. Using the LiDAR-derived $H$, Equation (2) allowed us to calculate the LiDAR-derived DBH. Figure 9c and d shows that the LiDAR estimation captured canonical forms of the field-derived distributions. LiDAR-derived and field-derived mean DBHs (Table IV) were not statistically different ($P = 0.12$ and 0.31 in Hinoki and Sugi, respectively; Welch's $t$-test). Departures in Figure 9c and d are the result of steeper tails on the left and right sides of the probability density function, resulting in the DBH distribution having negative kurtosis in both species. In Sugi, the tail on the left side of the function is flatter than the right side, resulting in negative skewness of the distribution.

The LiDAR-derived $A_{scat}/A_g$ obtained from Methods A–D were compared with $A_{scat}/A_g$ obtained from the field survey method (Table IV and Figure 10). In Methods A–C, the LiDAR-derived $A_{scat}/A_g$ of Hinoki was almost 0.9, while that of Sugi ranged from 0.85 to 1.00 relative to the field-derived value. In Method D, the numbers were 0.84 for Hinoki and 0.95 for Sugi. The results indicate that Method D is able to reproduce the actual $A_{scat}/A_g$ with an accuracy that was comparable with the other LiDAR methods.

## DISCUSSION

Kumagai *et al*. (2008, 2014) reported that the difference in ET among several sample plots in the same catchment was mainly determined by the variation in $A_{scat}/A_g$, which was affected by the slope position of each plot. The scaling step from the stand-level total sapwood area over ground area to catchment-level $A_{scat}/A_g$ includes a

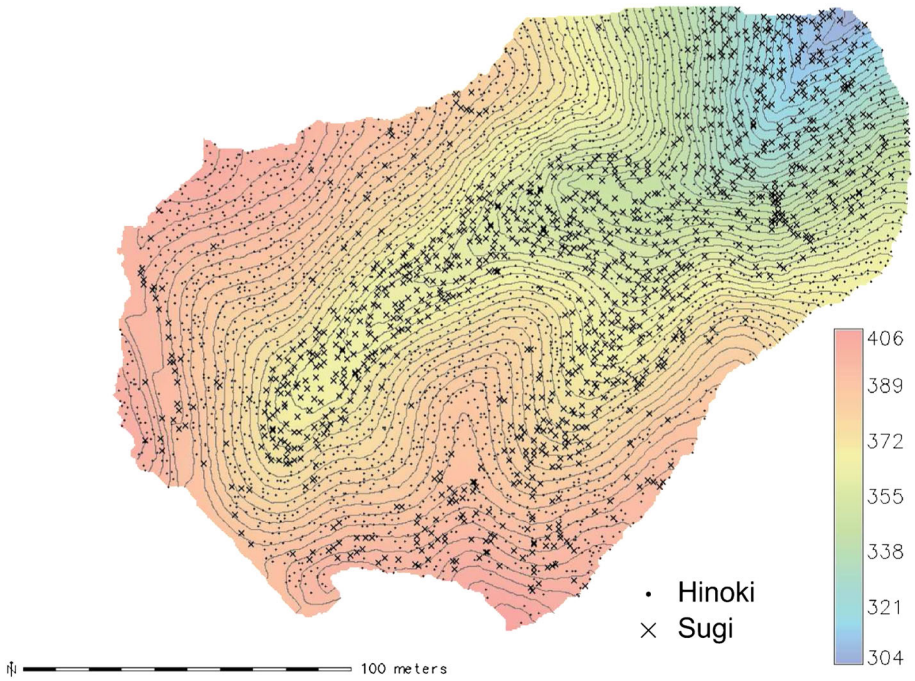


Figure 8. Distribution of the estimated *Chamaecyparis obtusa* (Hinoki) and *Cryptomeria japonica* (Sugi) tree apices in the catchment. Tree apices were detected using local maximum filtering on the digital surface model composed of the maximum pulse level in each grid. All tree apices were separated into the two species based on the criteria offered in this study

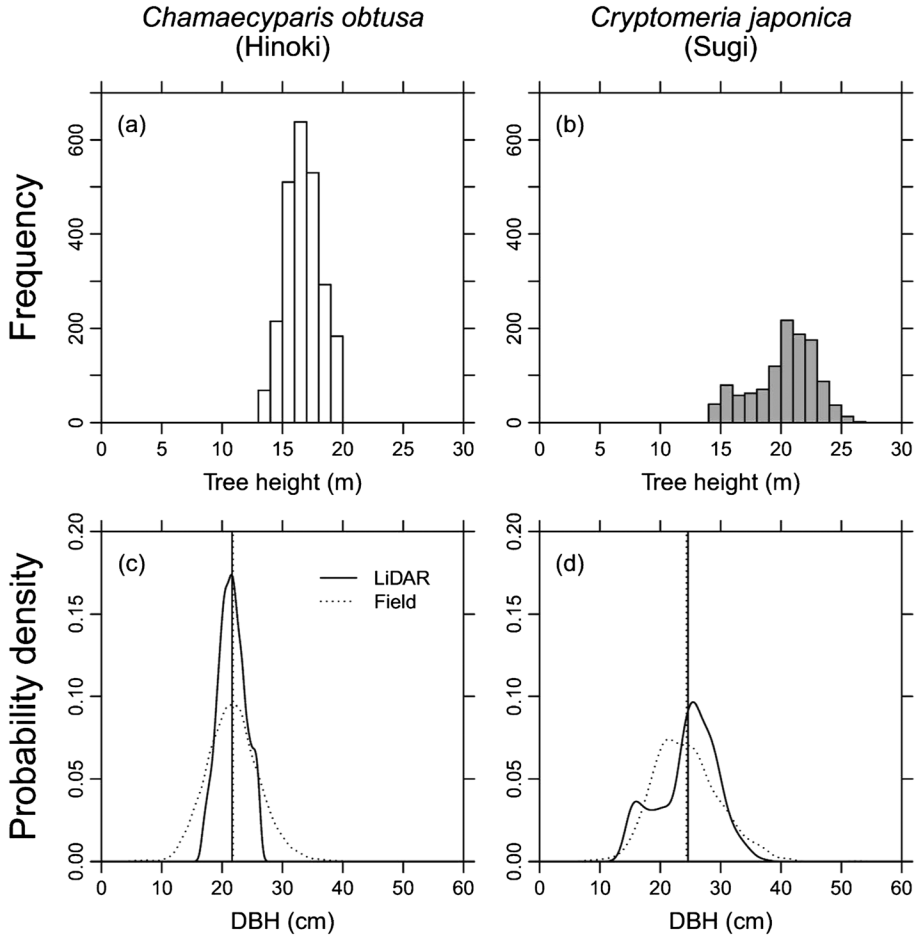


Figure 9. Histograms for LiDAR-derived height of tree apices for (a) Hinoki and (b) Sugi in the catchment. Probability density of diameter at breast height (DBH) estimated from LiDAR-derived $H$ is compared with field-derived DBH for (c) Hinoki and (d) Sugi. Vertical lines and dots indicted mean values

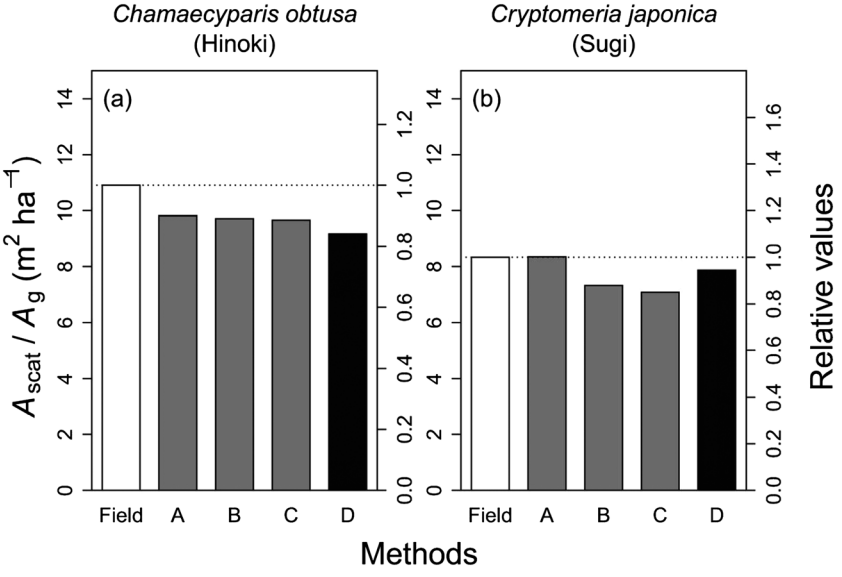


Figure 10. LiDAR-derived cumulative sapwood area divided by ground area ($A_{scat}/A_g$) in (a) Hinoki and (b) Sugi. Field-derived $A_{scat}/A_g$ (Field) was used as a reference value for the other $A_{scat}/A_g$ estimated with Methods A–D. Table IV presents values of $A_{scat}/A_g$

considerable amount of variation in stand density and sapwood area (e.g. Ford *et al*., 2007), and a field sampling campaign is inevitably limited in terms of the area covered by the tree census.

Here, our estimation of $A_{scat}$ with LiDAR was less influenced by slope position of the sample plots than that has been reported in other studies based on field surveys. Tree apices were identified evenly across the catchment area, and the windows for extracting species-specific characteristics of the canopy (i.e. USWs) can be established on slopes with various angles and aspects using GIS (Table III). Moreover, laser scanning from an airborne platform requires only a short time; for example, it took 1 hour to survey the entire area of the YEC including the nearby surrounding area. Thus, the LiDAR technology can be effective in monitoring $A_{scat}/A_g$ in a catchment of more than several hectares especially in mountainous areas. Moreover, the LiDAR enables monitoring $A_{scat}/A_g$ repeatedly, such as for planning the thinning and confirming the results throughout all stages of stand development.

*Variations in DBH versus $A_{stre}$ relationship*

Spatial variation in the DBH–$A_{stre}$ relationships within the catchment should not be a source of error in the $A_{scat}/A_g$ estimate. Practically, the use of the DBH–$A_{stre}$ relationship (Figure 4) is essential for estimating not only field-derived $A_{scat}/A_g$ but also the values obtained in Methods B–D. In reality, the DBH–$A_{stre}$ relationships varied between the partial plots in the same catchment, mainly because of their slope positions (Kumagai *et al*., 2007). However, we minimized the variation in DBH–$A_{stre}$ relationships among slope positions by conducting data collection across the entire area of the catchment.

We should choose an adequate DBH–$A_{stre}$ relationship according to the location of study site in Hinoki or the conditions for sapflow measurement in Sugi. In Figure 4, DBH–$A_{stre}$ relationships in the YEC were applied to those in the Miyazaki Experimental Forest in Kumagai *et al*. (2005b) for each species. Although data were obtained when the two plantations were of similar ages (42 and 51 years old in YEC and Miyazaki Experimental Forest, respectively), there was some degree of difference between the two studies. The difference in Hinoki could be induced by the variety of the subject tree species and/or site conditions. Sampling in Kumagai *et al*. (2005b) was conducted in the central mountain range (1150 m a.s.l.) on Kyushu Island where annual precipitation (3500 mm) was larger than in the YEC. We noted that that the curve of this study can be applied to Hinoki plantations around the headwaters of the Onga River in northern Kyushu area.

On the other hand, the difference in Sugi was caused by the difference in the estimating procedure for $A_{stre}$. The intermediate wood (i.e. white band) was not included in $A_{stre}$ in this study, while Kumagai *et al*. (2005b) included it. If the intermediate part is involved in determining $A_{stre}$, the curve of the DBH–$A_{stre}$ relationship in the YEC is identical to that of Kumagai *et al*. (2005b). Thus, we should choose the relationship of Sugi based on the location of the sensor probes for measuring sapflow rate. In summary, one should apply the relationship of Kumagai *et al*. (2005b) if sensor probes are placed across the depth of sapwood and the intermediate wood. On the other hand, the relationship obtained in this study should be used if the sensor probes were placed only across the SWD.

*Errors in LiDAR-derived values to estimate $A_{scat}/A_g$*

The LiDAR-derived $H$ appears to be reliable in this study. Some previous studies suggested that insufficient laser pulse density was likely to cause underestimations of $H$ and $N$ because of higher probability of failure to hit the tree apices (Persson *et al*., 2002; Gaveau and Hill, 2003). However, LiDAR-derived $H$ had an accuracy of better than 1 m in Hinoki (Hirata *et al*., 2009), and even in a Sugi plantation with a mean slope angle of approximately 38° (Takahashi *et al*., 2005). The present study carried out LiDAR data processes similar to that in the two previous studies. The grid size (0.5 m) in this study was somewhat larger than that in the previous two studies (0.25–0.33 m), resulting in a small number of interpolations of blank grids in DSMs. Laser pulse density (30 points $m^{-2}$) was higher than that of Takahashi *et al*. (2005) (8.80–15.60 points $m^{-2}$) and somewhat smaller than that of Hirata *et al*. (2009) (40.5 points $m^{-2}$), indicating high probability of tree apices hit by the laser pulses.

However, underestimation of $N$ seemed to lead to underestimations of $A_{scat}/A_g$ in the four LiDAR methods. LiDAR-derived $N$ were 0.92 and 0.88 of the true number in Hinoki and Sugi, respectively (Table IV), which indicates omission errors of approximately 9% averaged across the two species. Takahashi *et al*. (2005) showed that some small trees were not detected if the height and crown radius were smaller than the mean values of the sites. In principle, such errors in terms of omitting tree apices could occur in any LiDAR scans of a forest with a certain tree density, and the YEC was no exception.

The mutual error in the species identification might not significantly influence the estimation of $A_{scat}/A_g$ for each species. Separating tree apices into the two species was reasonably accurate. Local maxima after the species separation were plotted on the orthophoto of the catchment, which allowed us to check the consistency of the estimated species to actual species. Errors in species identification were 436 trees (17.9%) and 197

trees (17.2%) in the estimated Hinoki and Sugi populations, respectively. As described earlier, the omission errors occurred at a similar rate in the two populations (Table IV), and the mean value of LiDAR-derived DBH was comparable with that of field-derived DBH (Figure 9c and d). These results suggest that a large number of small Sugi trees were assigned as Hinoki, while a small number of large Hinoki trees were determined to be Sugi. However, >82% of all tree apices represented the correct species; thus, the difference in tree size composition between the field-derived and LiDAR-derived populations might have a minor effect on the $A_{scat}/A_g$ estimates for each species. Our threshold values in the criteria may not be universally applied to other plantations, because the $H$ and $\sigma$ are sensitive to stand age and site quality. However, our approach, which included making examination windows (i.e. USWs) inside the DSMs, can generally be applied to other plantations, where parts of the area are composed of homogeneous species.

*Field campaigns required for estimating $A_{scat}/A_g$ in LiDAR methods*

Method A is the most simple and accurate but does not make the best use of remote-sensing LiDAR technology. The LiDAR-derived $H$ was directly converted to each tree's $A_{stre}$ in Method A. Resultant $A_{scat}/A_g$ seemed to provide the best estimate of the field-derived $A_{scat}/A_g$ among the four LiDAR methods. However, obtaining the $H$–$A_{stre}$ relationship (Figure 3b) again requires labour-intensive field campaigns for every site. For example, 47 and 27 points of Hinoki and Sugi, respectively (Figure 3b), required 296 increment borer samples in total. Such a large number of stem injuries is not acceptable in normal commercial plantations.

Method B and C also required considerable measurements in field. Conversion from LiDAR-derived $H$ to DBH is a necessary first step for estimating $A_{scat}$. The $H$–DBH plots had many scattered points (Figure 3a), and thus, the derived Equation (2) did not have a very high prediction capability. The value gained through increasing the number of samples would not justify the increased costs of field observations. In this study, LiDAR-derived mean DBH was almost consistent with field-derived mean DBH in both species (Figure 9c and d), so that Equation (2) may not be a major source of error. Nevertheless, this consistency would not be expected in other sites where intensive field surveys cannot be conducted. Obviously, Methods A–C require extensive field campaigns to prepare either an 'ad hoc' DBH–$A_{stre}$ or DBH–$H$ relationship for the objective site. Thus, Method A–C cannot be used as standard, minimal labour procedure, for deducing $A_{scat}/A_g$ at other sites.

*Applying SDMD to estimate $A_{scat}/A_g$*

Method D reproduced the field-derived $A_{scat}$ reasonably well (Table IV). Note that only LiDAR-derived $H$ and $N$, and the 'ready-made' SDMD with a DBH-$A_{stre}$ curve are required for estimating $A_{scat}$ under Method D. The LiDAR-derived tree density and mean $H$ in a catchment can be used to parameterize average stand-level models in SDMD with no scale gaps. Moreover, LiDAR can detect the tree apices across more than several hectares; clearly, collecting this type of data through field observation is not practical. In this sense, Method D is the most appropriate among the four methods offered here.

The robustness of $A_{scat}/A_g$ estimation with Method D was elucidated through a sensitivity analysis (Figure 11a). As mentioned earlier, LiDAR-derived $N$ inevitably underestimate the true $N$, which will be a major source of error in LiDAR-derived $A_{scat}/A_g$. Changing $A_{scat}/A_g$ was examined through the manipulation of $N$ under a fixed mean tree height (16.7 m and 20.3 m in Hinoki and Sugi, respectively). Where LiDAR-derived $N$ equaled the field-derived $N$ (i.e. relative $N = 1.0$), the relative $A_{scat}/A_g$ was predicted to be 0.87 in Hinoki and 1.00 in Sugi. The Sugi case is an ideal example for showing the robustness of $A_{scat}/A_g$ estimation when Method D is used in uninvestigated plantations. We should be able to realize less than 8% underestimation of $A_{scat}/A_g$ within the range of 0–20% reduction in LiDAR-derived $N$ relative to actual values. In the case of Hinoki, the $A_{scat}/A_g$ was underestimated even at a relative $N = 1.0$, because the SDMD somewhat underestimates DBH in the YEC. However, underestimation of $A_{scat}/A_g$ was less than 20% within the range of 0–20% reduction in $N$. Although SDMDs will not necessarily predict the actual DBH in some plantations, the errors never diminish the potential usage of the diagrams. SDMDs are able to predict stand-average DBH of the plantations where the investigator cannot conduct field surveys.

The reduction in relative $A_{scat}/A_g$ is gradual in comparison with the reduction in relative $N$ (Figure 11a), resulting from a certain amount of compensation by mean DBH intensified with decreasing $N$ (Figure 11b). In Sugi, the mean DBH (hence, mean $A_{stre}$) was overestimated in the process of Method D, but the intrinsic underestimation of $N$ compensates the mean $A_{stre}$ overestimation, resulting in reasonable reproduction of $A_{scat}/A_g$ (Figure 10). The same compensation occurred in Hinoki, although $A_{scat}/A_g$ was underestimated to a greater extent because SDMD underestimated mean DBH in the YEC. The estimates of mean DBH increase with decreasing $N$ in a given stand area in SDMD (Figure 11b). One of the principles of SDMD is the natural law of competition-density effect (Kira *et al.*, 1953), which is expressed by

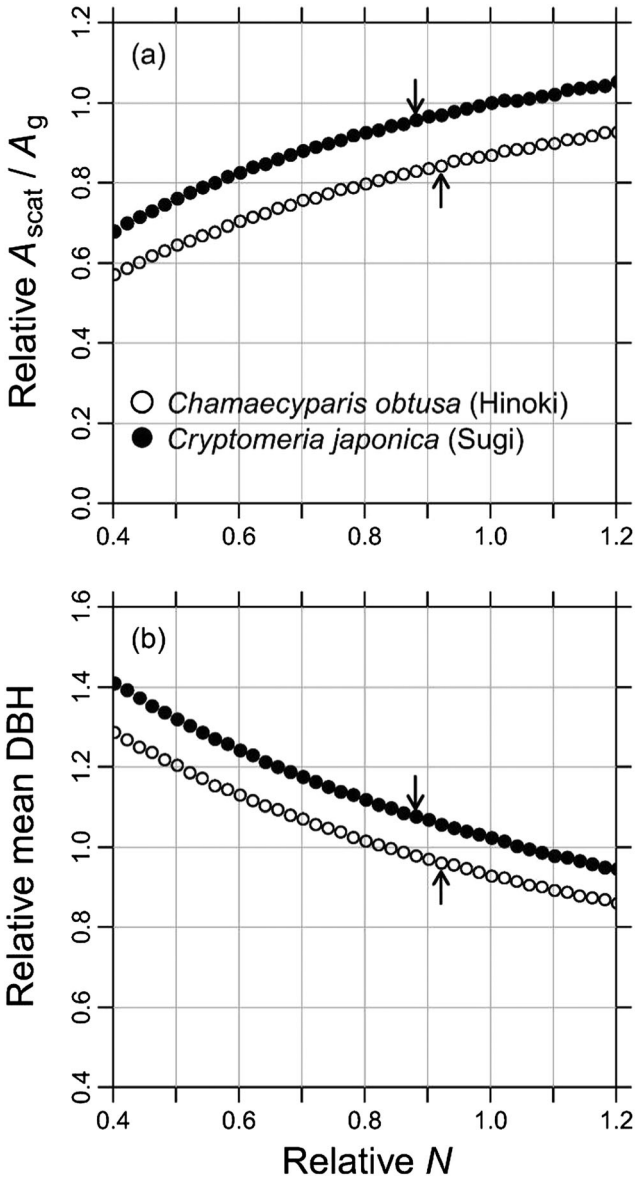


Figure 11. Sensitivity analysis of (a) LiDAR-derived cumulative sapwood area divided by ground area ($A_{scat}/A_g$) and (b) LiDAR-derived mean diameter at breast height (DBH). The LiDAR-derived tree number ($N$) is manipulated under a fixed mean tree height (16.7 and 20.3 m in Hinoki and Sugi, respectively). The LiDAR-derived $A_{scat}/A_g$ and the mean DBH were calculated with Method D. The values were relative to the corresponding field-derived values. Arrows indicate the relative $A_{scat}/A_g$ or the relative mean DBH at underestimated $N$ (0.92 and 0.88 in Hinoki and Sugi, respectively) estimated by the LiDAR technique in the catchment

using the equation as $1/w = A\rho + B$, where $w$ is mean biomass per plant, $\rho$ is the number of plants per unit area, and A and B are constants. The reciprocal relationship can be also applied to the relationships between stand density and basal area (hence, DBH) in conifer plantations (Ando, 1968).

At a landscape level, the measure of $A_{scat}/A_g$ might be influenced by the site quality including atmospheric factors such as solar radiation and atmospheric evaporative demand. The $A_{scat}/A_g$ is closely related to $E_{cat}$ (Equation [1]), which is an important component of forest evapotranspiration (ET). The measured annual ET has been reported to be conservative at each site (e.g. Roberts, 1983; Kosugi and Katsuyama, 2007), and annual ET in the 43 catchments across Japan had a linear relationship with mean annual air temperature (Komatsu *et al*., 2008).

We can recommend use of the more efficient Method D to estimate $A_{scat}/A_g$, because the accuracy was at a level similar to the labour-intensive Methods A–C. The degree of variation in the $A_{scat}/A_g$ estimate between the field method and the LiDAR methods (Figure 10) was comparable with the degree of variation in $J_s$ estimates in a catchment (approximately ±10%; Kume *et al*., 2009; Kumagai *et al*., 2014). To estimate $E_{cat}$ with greatest accuracy, we have to consider not only how $J_s$ was measured but also consider how the $A_{scat}/A_g$ was estimated considering the available funds for such estimations. Use of airborne LiDAR with existing SDMDs is a less labour-intensive method for evaluating $A_{scat}/A_g$. Future work could also couple LiDAR measurements to quantify $E_{cat}$ with field-based measurements of precipitation partitioning (i.e. throughfall, stemflow and interception; Saito *et al*., 2013) from representative tree species. The effects of species-specific canopy structure on the partitioning (such as Levia *et al*., 2015) could be used with LiDAR measurements of canopy structure on a catchment scale, to develop a more complete understanding of the hydrologic cycle of these plantations.

## CONCLUSION

Four methods were examined for estimating $A_{scat}$ using LiDAR-derived data. Hinoki and Sugi were identified reasonably well employing the criteria of tree height and canopy roughness in the USWs. The field-derived $H$–$A_{stre}$ and $H$–DBH relationships were scattered despite intensive field campaigns. The LiDAR technique underestimated $N$, which caused underestimation of $A_{scat}/A_g$. When SDMDs are used for estimating $A_{scat}/A_g$ of uninvestigated forests, we should be able to realize less than 8% underestimation of $A_{scat}/A_g$ within the range of 0–20% reduction in $N$ relative to actual values. We suggest that coupling LiDAR-derived $H$ and $N$ with SDMDs requires the least amount of labour and provides an effective method for estimating $A_{scat}/A_g$.

## ACKNOWLEDGEMENTS

This study was conducted primarily under the project 'Development of innovative technologies for increasing in watershed runoff and improving river environment by

the management practice of devastated forest plantation' funded by Core Research for Evolutional Science and Technology (CREST) of the Japan Science and Technology (JST). We are grateful to Drs Y. Onda, H. Kato, K. Nanko, A. Hirata, Y. Komatsu, T. Kasahara, N. Kobayashi, S. Hamada, T. Nonoda, D. F. Levia and T. Gomi for their support of field measurements and critical advice. TS and TK were supported by a grant from the Japanese Ministry of Agriculture, Forestry and Fisheries.

## ABBREVIATIONS

| | |
|---|---|
| $A_{scat}/A_g$ | Cumulative sapwood area over the catchment area ($m^2\,ha^{-1}$) |
| $A_{stre}$ | Sapwood area of a single tree in a stem cross section ($m^2$) |
| BRD, $L_{BRD}$ | Bark depth in the stem cross section (cm) |
| DBH, $D$ | Diameter at breast height (cm; at approximately 1.2 m) |
| DTM | Digital terrain map |
| $DSM_{max}$ | Digital surface map composed of the grids with the maximum elevation among the first returns of the laser pulse fallen in each grid |
| $DSM_{mean}$ | Digital surface map composed of the grids with mean elevation among the first returns of the laser pulse fallen in each grid |
| $E_{cat}$ | Transpiration rate in the catchment ($mm\,d^{-1}$) |
| Field | Field-derived $A_{scat}/A_g$ |
| GIS | Geographic information system |
| $H$ | Individual tree height (m) |
| $J_s$ | Sap flux density ($m^3\,m^{-2}\,d^{-1}$) |
| LiDAR | Light detection and ranging |
| LMF | Local maximum filtering |
| $N$ | The number of trees |
| $\sigma$ | Population standard deviation of the height of 29 grids in the hypothetical canopy circle in $DSM_{mean}$ |
| SDMD | Stand density management diagram |
| SWD, $L_{SWD}$ | Sapwood depth in the stem cross section (cm) |
| USW | Uniform species window |
| YEC | Yayama experimental catchment |

## REFERENCES

Alsheimer M, Köstner B, Falge E, Tenhunen JD. 1998. Temporal and spatial variation in transpiration of Norway spruce stands within a forested catchment of the Fichtelgebirge, Germany. *Annals of Forest Science* **55**: 103–123.

Ando T. 1968. Ecological studies on the stand density control in even-aged pure stand. *Bulletin of the Government Forest Experiment Station (Tokyo)* **210**: 1–153. (in Japanese with English summery)

Ford CR, Hubbard RM, Kloeppel BD, Vose JM. 2007. A comparison of sap flux-based evapotranspiration estimates with catchment-scale water balance. *Agricultural and Forest Meteorology* **145**: 176–185.

Gaveau DLA, Hill RA. 2003. Quantifying canopy height underestimation by laser pulse penetration in small-footprint airborne laser scanning data. *Canadian Journal of Remote Sensing* **29**(5): 650–657.

GRASS Development Team. 2012. Geographic resources analysis support system (GRASS) software. Open Source Geospatial Foundation Project. http://grass.osgeo.org [Accessed February 18, 2014].

Hirata Y, Furuya N, Suzuki M, Yamamoto H. 2009. Airborne laser scanning in forest management: individual tree identification and laser pulse penetration in a stand with different levels of thinning. *Forest Ecology and Management* **258**: 752–760.

Hyyppä J, Lehikoinen M, Inkinen M. 2001. A segmentation-based method to retrieve stem volume estimates from 3-D tree height models produced by laser scanners. *IEEE Transactions on Geoscience and Remote Sensing* **39**(5): 969–975.

Inoue Y, Miyahara H. 1954. On the yield-table of Sugi stand at Kasuya University Forest. *Reports of the Kyushu University Forests* **2**: 15–50. (in Japanese)

Japan Forest Agency. 1957. Yield table of Hinoki stands in Kyushu-area. The Ministry of Agriculture, Forestry and Fisheries of Japan, Tokyo. (in Japanese)

Japan Forest Agency. 2013. Annual report on forest and forestry in Japan: fiscal year 2013. The Ministry of Agriculture, Forestry and Fisheries of Japan, Tokyo, pp. 85. (in Japanese)

Kawana A. 1992. *Forestation in Forestry*, 3rd edn. Asakura: Tokyo, pp. 101. (in Japanese)

Kira T, Ogawa H, Sakazaki N. 1953. Intraspecific competition among higher plants. I. Competition-density-yield interrelationship in regularly dispersed population. *Journal of the Institute of Polytechnics (Osaka City University) Series* **4**: 1–16.

Komatsu H, Maita E, Otsuki K. 2008. A model to estimate annual forest evapotranspiration in Japan from mean annual temperature. *Journal of Hydrology* **348**: 330–340.

Kosugi Y, Katsuyama M. 2007. Evapotranspiration over a Japanese cypress forest. II. Comparison of the eddy covariance and water budget methods. *Journal of Hydrology* **334**: 305–311.

Kumagai T, Aoki S, Nagasawa H, Mabuchi T, Kubota K, Inoue S, Utsumi Y, Otsuki K. 2005a. Effects of tree-to-tree and radial variations on sap flow estimates of transpiration in Japanese cedar. *Agricultural and Forest Meteorology* **135**: 110–116.

Kumagai T, Nagasawa H, Mabuchi T, Ohsaki S, Kubota K, Kogi K, Utsumi Y, Koga S, Otsuki K. 2005b. Sources of error in estimating stand transpiration using allometric relationships between stem diameter and sapwood area for *Cryptomeria japonica* and *Chamaecyparis obtusa*. *Forest Ecology and Management* **206**: 191–195.

Kumagai T, Aoki S, Shimizu T, Otsuki K. 2007. Sap flow estimates of stand transpiration at two slope positions in a Japanese cedar forest watershed. *Tree Physiology* **27**: 161–168.

Kumagai T, Tateishi M, Shimizu T, Otsuki K. 2008. Transpiration and canopy conductance at two slope positions in a Japanese cedar forest watershed. *Agricultural and Forest Meteorology* **148**: 1444–1455.

Kumagai T, Tateishi M, Miyazawa Y, Kobayashi M, Yoshifuji N, Komatsu H, Shimizu T. 2014. Estimation of annual forest evapotranspiration from a coniferous plantation watershed in Japan (1): water use components in Japanese cedar stands. *Journal of Hydrology* **508**: 66–76.

Kume A, Tsuruta K, Komatsu H, Kumagai T, Higashi N, Shinohara Y, Otsuki K. 2009. Effects of sample size on sap flux-based stand-scale transpiration estimates. *Tree Physiology* **30**: 129–138.

Kuroda K, Yamashita K, Fujiwara T. 2009. Cellular level observation of water loss and the refilling of tracheids in the xylem of *Cryptomeria japonica* during heartwood formation. *Trees* **23**: 1163–1172.

Lefsky MA, Cohen WB, Parker GG, Harding D. 2002. Lidar remote sensing for ecosystem studies. *BioScience* **52**(1): 19–30.

Levia DF, Näthe MK, Bischoff S, Richter S, Legates DR. 2015. Differential stemflow yield from European beech saplings: the role of individual canopy structure metrics. *Hydrological Processes* **29**: 43–51.

 

Nagai S, Taniguchi Y. 2001. Air permeability in wood of *Cryptomeria japonica* D. Don: air permeability in heartwood, white zone wood and sapwood in green logs. *Zairyo* **50**: 409–414. (in Japanese with English summary)

Nagai S, Utsumi Y. 2012. The function of intercellular spaces along the ray parenchyma in sapwood, intermediate wood, and heartwood of *Cryptomeria japonica* (Cupressaceae). *American Journal of Botany* **99**: 1553–1561.

Nagakura J, Shigenaga H, Akama A, Takahashi M. 2004. Growth and transpiration of Japanese cedar (*Cryptomeria japonica*) and Hinoki cypress (*Chamaecyparis obtusa*) seedlings in response to soil water content. *Tree Physiology* **24**: 1203–1208.

Newton PF. 1997. Stand density management diagrams: review of their development and utility in stand-level management planning. *Forest Ecology and Management* **98**: 251–265.

Nobuchi T, Harada H. 1983. Physiological features of the "white zone" of sugi (*Cryptomeria japonica* D. Don) – cytological structure and moisture content. *Mokuzai Gakkaishi* **29**: 824–832.

Ohashi H, Motegi Y, Yasue M. 1985. Water distribution and water alleyway in the living stem of *Cryptomeria japonica*. *Research Bulletin of the Faculty College of Agriculture Gifu University* **50**: 111–129.

Pataki DE, Oren R. 2003. Species differences in stomatal control of water loss at the canopy scale in a mature bottomland deciduous forest. *Advances in Water Resources* **26**: 1267–1278.

Persson A, Holmgren J, Söderman U. 2002. Detecting and measuring individual trees using an airborne laser scanner. *Photogrammetric Engineering and Remote Sensing* **68**: 925–932.

Popescu SC, Wynne RH, Nelson RF. 2002. Estimating plot-level tree heights with lidar: local filtering with a canopy-height based variable window size. *Computers and Electronics in Agriculture* **37**: 71–95.

R Core Team. 2013. R: a language and environment for statistical computing. R Foundation for Statistical Computing, Vienna, Austria. http://www.R-project.org/ [Accessed February 15, 2014].

Roberts J. 1983. Forest transpiration: a conservative hydrological process? *Journal of Hydrology* **66**: 133–141.

Roberts S, Vertessy R, Grayson R. 2001. Transpiration from *Eucalyptus sieberi* (L. Johnson) forests of different age. *Forest Ecology and Management* **143**: 153–161.

Roth BE, Slatton KC, Cohen MJ. 2007. On the potential for high-resolution lidar to improve rainfall interception estimates in forest ecosystems. *Frontiers in Ecology and the Environment* **5**: 421–428.

Saito T, Matsuda H, Komatsu M, Xiang Y, Takahashi A, Shinohara Y, Otsuki K. 2013. Forest canopy interception loss exceeds wet canopy evaporation in Japanese cypress (Hinoki) and Japanese cedar (Sugi) plantations. *Journal of Hydrology* **507**: 287–299.

Takahashi T, Yamamoto K, Senda Y, Tsuzuku M. 2005. Estimating individual tree heights of sugi (*Cryptomeria japonica* D. Don) plantations in mountainous areas using small-footprint airborne LiDAR. *Journal of Forest Research* **10**: 135–142.

Vierling KT, Vierling LA, Gould WA, Martinuzzi S, Clawges RM. 2008. Lidar: shedding new light on habitat characterization and modeling. *Frontiers in Ecology and the Environment* **6**: 90–98.

Wilson KB, Hanson PJ, Mulholland PJ, Baldocchi DD, Wullschleger SD. 2001. A comparison of methods for determining forest evapotranspiration and its components: sap-flow, soil water budget, eddy covariance and catchment water balance. *Agricultural and Forest Meteorology* **106**: 153–168.

Wullschleger SD, Hanson PJ, Todd DE. 2001. Transpiration from a multi-species deciduous forest as estimated by xylem sap flow techniques. *Forest Ecology and Management* **143**: 205–213.

Zimmermann R, Schulze E-D, Wirth C, Schulze E-E, McDonald KC, Vygodskaya NN, Ziegler W. 2000. Canopy transpiration in a chronosequence of Central Siberian pine forests. *Global Change Biology* **6**: 25–37.

 